On the origin of the significant difference in lithiation behavior between silicon and germanium
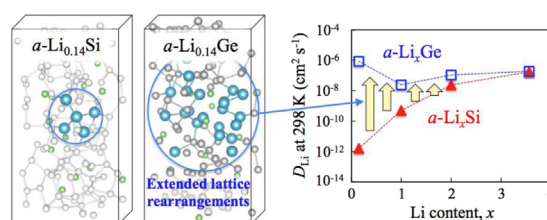
Chia-Yun Chou [a], Gyeong S. Hwang [a,b,]*

[a] Materials Science and Engineering Program, University of Texas at Austin, Austin, TX 78712, USA
[b] Department of Chemical Engineering, University of Texas at Austin, Austin, TX 78712, USA

HIGHLIGHTS

- We examine and compare the lithiation behavior of Si and Ge using DFT calculations.
- Li diffusivity is greater and less concentration-dependent in Ge as compared to Si.
- Li diffusion is subject to Li—host interaction and host lattice rigidity/dynamics.
- We reveal the origin of the superior rate performance of Ge-based anodes.
- High performance anodes can be designed via fine-tuning of Si—Ge alloys.

GRAPHICAL ABSTRACT

ABSTRACT

Silicon and germanium are both recognized as a promising anode material for high-energy lithium-ion batteries. Si is best known for its superior energy storage capacity, while Ge exhibits better rate capability and cycleability. To better understand the underlying reasons behind their lithiation behavior differences, particularly the enhanced Li transport in Ge, we examine and compare Li-host lattice interactions and dynamics using density functional theory calculations. At the onset of lithiation, an isolated Li interstitial is found to form polar covalent bonds with four nearest host atoms, while the degree of covalency is noticeably greater for Li—Si than Li—Ge bonds. The relatively stronger Li—Si interaction, along with the stiffer Si lattice tend to be responsible for the suppressed Li mobility ($D_{Li} = 10^{-13}$ cm^2 s^{-1}) in c-Si, as compared to the c-Ge case ($D_{Li} = 10^{-11}$ cm^2 s^{-1}). With continued lithiation, D_{Li} in a-Li$_x$Si increases significantly from 10^{-12} to 10^{-7} cm^2 s^{-1} ($x = 0.14–3.57$); contrarily, D_{Li} in a-Li$_x$Ge is around 10^{-7} cm^2 s^{-1} and less concentration dependent. Our analysis shows that the rapid Li diffusion in a-Li$_x$Ge is directly related to the facile atomic rearrangements of host Ge atoms even at the early stages of lithiation.

© 2014 Elsevier B.V. All rights reserved.

1. Introduction

Li-ion batteries (LIBs) have received tremendous attention as they power a wide range of applications from portable devices, electric vehicles to various renewable energy systems [1–3]. Currently, the most adopted anode material is graphite, which has good cycleability but the dendrite formation raises safety concerns

* Corresponding author. Materials Science and Engineering Program, University of Texas at Austin, Austin, TX 78712, USA, Tel.: +1 512 471 4847; fax: +1 512 471 7060.

    E-mail address: gshwang@che.utexas.edu (G.S. Hwang).

and the capacity is rather limited (372 mAh g^{-1}) especially at high charge/discharge rates. Therefore, in order to satisfy the ever-increasing energy density/power capability requirements and stringent safety standards, there is an imminent need to find new electrode materials with superior lithiation properties. Among the alternatives considered, Si stands out the most because of its impressive capacity (4200 mAh g^{-1} for Li$_{22}$Si$_5$ [4,5]), safe thermodynamic potential and abundance. Second only to Si, Ge has a relatively high theoretical capacity of 1624 mAh g^{-1} (Li$_{22}$Ge$_5$ [6]), a higher electrical conductivity compared to Si [7], and a superior rate capability, up to 1000 C (full lithiation in 1/1000 h) [6]. However, the understanding and development of Ge-based anodes have gained much less attention likely because of its higher price relative to Si.

Being in the same column in the periodic table, Si and Ge share many similarities, including the disadvantages of undergoing large structural changes and volume expansion upon lithiation, which can consequently lead to early capacity fading. To overcome this drawback, many ongoing studies have focused on utilizing Si and Ge of different forms, such as thin films [8–12], nanoparticles [13,14], nanowires [15–18], and alloys/composites with active/inactive elements [19–22]. In both Si and Ge cases, nanostructuring seems to have positive impacts on enhancing the rate capability and reducing/preventing electrode pulverization, thereby improving the cycleability. In comparison to Si, Ge of comparable nano-architecture is able to withstand much faster charging rates with noticeably less crack formation [23,24]. Furthermore, there appears to be subtle differences in their responses to electrochemical lithiation/delithiation, as demonstrated by recent *in-situ* characterization [24]. On the theoretical side, there have been many studies employing density functional theory (DFT) to examine Li incorporation in Si (crystalline/amorphous bulks [25–27] and nanowires [28,29]) and a few on Ge [30–32]. Nonetheless, the fundamental understanding regarding the nature and origin of their dissimilar responses to lithiation is still limited; to the best of our knowledge, no atomistic study has been reported to investigate the likely overlooked differences between Si and Ge as anode material, especially regarding their lithiation dynamics.

In this paper, on the basis of DFT calculations, we examine how Li diffusion is affected by its interaction with the pure Si and Ge matrices, analyze the dynamic behaviors of Li as well as the host lattice atoms, and look into the impacts of Ge-alloying on anode performance. The fundamental findings explain the origin of the lithiation behavior differences between Si and Ge, particularly the significantly enhanced Li transport in Ge, and thus assist the rational design of the next-generation high performance Si- and Ge-based anodes.

2. Computational methods

The calculations reported herein were performed on the basis of density functional theory (DFT) within the generalized gradient approximation (GGA-PW91) [33], as implemented in the Vienna Ab-initio Simulation Package (VASP) [34–36]. Spin polarization of the Li–Si (Ge) system was also examined, but appears to be unimportant. The projector augmented wave (PAW) method with a planewave basis set was employed to describe the interaction between ion cores and valence electrons. The PAW method is, in principle, an all-electron frozen-core approach that considers exact valence wave functions. Valence configurations employed are as follows: $1s^2 2s^1$ for Li, $3s^2 3p^2$ for Si and $4s^2 4p^2$ for Ge. An energy cutoff of 350 eV was applied for the planewave expansion of the electronic eigenfunctions. The crystalline Si (Ge) host was modeled using a 216-atom supercell with a fixed lattice constant of 5.457 (5.777) Å; the effect of volume relaxation was also checked, and

turns out to be unimportant as the 216-atom supercell is large enough to accommodate one Li atom with no significant volume change (less than 1%). For geometry optimization, all atoms were fully relaxed using the conjugate gradient method until residual forces on constituent atoms become smaller than 5×10^{-2} eV Å^{-1}, and a $(2 \times 2 \times 2)$ k-point mesh in the scheme of Monkhorst–Pack was used for the Brillouin zone sampling [37]. Diffusion pathways and barriers were determined using the climbing-image nudged elastic band method with eight intermediate images for each hopping step.

The model structures of amorphous a-Li$_x$M alloys (M = Ge and Si$_{1-y}$Ge$_y$) were created using ab initio molecular dynamics (AIMD) simulations based on the atomic configurations of a-Li$_x$Si alloys that were previously generated using the combined modified embedded atom method (MEAM) and AIMD simulations (see Refs. [31,38] for detailed computational methods). The interaction between Li and Ge is very similar to that with Si, and their lithiated phases tend to share many structural similarities [31,40,41]; therefore, the a-Li$_x$Si structure is likely a good starting configuration for the a-Li$_x$M structure. The Si atoms (in a-Li$_x$Si) were replaced by Ge atoms accordingly to achieve desired composition ratios; the replacement sites were carefully chosen to ensure homogeneous atomic mixing. The model structures, each containing 128 atoms, were then annealed at 300 K for 1.5 ps with a time step of 1 fs to allow sufficient atomic rearrangement (the annealing temperature was controlled via velocity rescaling), followed by geometry optimization using a $(2 \times 2 \times 1)$ k-point mesh. Periodic boundary conditions were employed in all three directions, and for each composition three independent samples were considered. This approach can provide reasonable Li–M amorphous structures at significantly reduced computational burden compared to starting with crystalline initial configurations. Finally, for diffusivity calculations, AIMD simulations of 8 ps duration with a time step of 1 fs were carried out at appropriate temperatures controlled via Nose–Hoover thermostat.

3. Results and discussion

We first examined how the room-temperature diffusivity of Li varies with Li content (x) in a-Li$_x$Si alloys using AIMD simulations

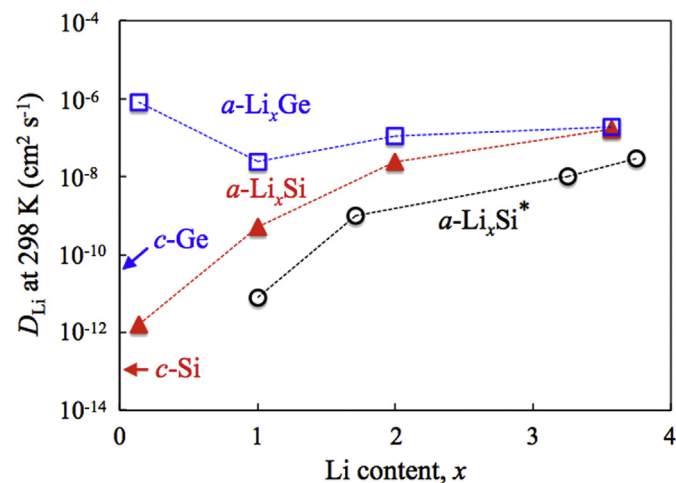**Fig. 1.** Predicted diffusivity of Li (D_{Li}) in a-Li$_x$Si and a-Li$_x$Ge using AIMD simulations at 298 K. The predicted D_{Li} values for single Li diffusion in c-Si [42] and c-Ge [31] are indicated by red and blue arrows, respectively. For comparison, D_{Li} values calculated by MD simulations with an embedded atom method interatomic potential are indicated by * [45]. (For interpretation of the references to color in this figure legend, the reader is referred to the web version of this article.)

[Fig. 1]. Here, a-Li$_x$Si alloys were considered, instead of their crystalline counterparts, because Si lithiated beyond the first charge cycle is most likely to remain in the amorphous state due to the sizable kinetic barrier for recrystallization at room temperature [8,39]. For each alloy, three samples are averaged to calculate the mean-square displacements (MSD) of Li atoms at each temperature; MSD = $|R_i(t) - R_i(0)|^2$, where $R_i(t)$ is the position of atom i at time t. Based on the MSD profiles, D_{Li} values are obtained using the Einstein relation, $D = <MSD>/6t$; the angular bracket denotes ensemble average over the AIMD interval. The MD duration of 8 ps appears to be sufficient to obtain well-converged results; disregarding the first 2 ps, linear fits over a time interval of the following 6 ps yield the D_{Li} values [39]. Using these calculated D_{Li} values at different temperatures, an Arrhenius plot of ln(D_{Li}) versus $1000/T$ is constructed based on $D = D_0 \exp(-E_a/kT)$ as shown in Fig. S1; the estimated prefactor D_0, diffusion barrier E_a, and room-temperature diffusivity D_{Li} values are summarized in Table S1.

Several observations can be made based on the above calculation results. Firstly, in comparison to Li diffusion in c-Si (where E_a and D_0 are predicted to be 0.62 eV and 3.18×10^{-3} cm^2 s^{-1}, respectively [42]), the E_a in a-Li$_x$Si is relatively smaller and becomes progressively more so with increasing Li contents. The reduction of E_a indicates Li can diffuse more easily in a-Li$_x$Si of larger x, which is not surprising given that the Si host matrix would be softened and undergo significant disintegration during lithiation [39,43]. Secondly, contrary to highly concentration-sensitive E_a, D_0 tends to be less affected by compositional changes and remain relatively constant around 10^{-3} cm^2 s^{-1}. Note that our predicted D_0 values are indeed comparable with the prediction based on harmonic transition state theory; according to which, $D_0 = \nu_0 a^2 \exp(-\Delta S/k)$, assuming ΔS (the entropy difference between the diffusing atom at the saddle point and the initial equilibrium state) is close to zero, ν_0 (the attempt frequency) $\approx 10^{13}$ s^{-1} and a (the distance between adjacent hopping sites) $\approx 10^{-8}$ cm, D_0 would be on the order of 10^{-3} cm^2 s^{-1} [44]. Lastly, manifested by the virtually unchanging D_0 and the decreasing E_a in the exponential term, D_{Li} in a-Li$_x$Si can rise by orders of magnitude with increasing x, from $\times 10^{-12}$ cm^2 s^{-1} ($x = 0.14$) to $\times 10^{-7}$ cm^2 s^{-1} ($x = 3.57$). Such trend has also been demonstrated by recent MD simulations although some discrepancies may appear due to different choices of interatomic potentials [45].

Next, same analyses are carried out to examine Li diffusivity in a-Li$_x$Ge alloys of varying Li contents [Fig. 1]. In c-Ge, taking $E_a = 0.44$ eV (as predicted from our previous work [31]) and assuming $D_0 = 10^{-3}$ cm^2 s^{-1}, the estimated D_{Li} ($\approx 10^{-11}$ cm^2 s^{-1}) at room temperature is about 10^2 times larger than that in c-Si. Unlike the Si case, D_{Li} in Ge is found to increase and plateau rapidly with lithiation; interestingly, the predicted D_{Li} values in a-Li$_{0.14}$Ge and a-Li$_{3.57}$Ge are of the same order ($\times 10^{-7}$ cm^2 s^{-1}). Our results suggest that, in the lithiated Ge matrices, D_{Li} tends to be less concentration-sensitive (as compared to the Si case) while Li diffusion can be extremely facile even during the early stages of lithiation. This difference in lithiation behavior between a-Li$_x$Ge and a-Li$_x$Si becomes progressively smaller with increasing Li contents, and the predicted D_{Li} values are both on the order of 10^{-7} cm^2 s^{-1} when $x = 3.57$. In the following sessions, to better understand the origin of the significant enhancement of Li diffusivity in Ge, particularly at the early stages of lithiation, we analyzed the interaction of Li with the host matrix as well as the dynamic behavior of host lattice atoms.

3.1. The interaction of Li with c-Si and c-Ge host matrices at 0 K

In both c-Si and c-Ge, the tetrahedral (T) site has been identified to be energetically the most favorable interstitial site for a Li atom, which may undergo migration by jumping between adjacent T-sites via the hexagonal (H) transition site [42]. Despite the

structural similarities, the predicted diffusion barrier ($E_a = 0.44$ eV) in c-Ge is considerably lower than 0.62 eV in c-Si. The difference in E_a could be attributed to two factors; (i) the flexibility of the host lattice to expand and allow Li passing though [31], and (ii) the interaction between the Li and host atoms, i.e., a greater E_a would be expected if the diffusing Li interstitial interacts more strongly with neighboring host atoms in the minimum-energy T state (relative to the transition H state).

It is well known that the Ge lattice is more flexible than the Si lattice, as demonstrated by its relatively lower bulk modulus ($B_{Ge} = 57$ GPa vs. $B_{Si} = 91.3$ GPa) [31,39]. In addition, our calculation shows that the restoring force acting on a Ge atom displaced from its equilibrium position is much smaller as compared to the Si case. For instance, as summarized in Table S2, the calculated restoring force for a selected Ge (Si) atom upon 0.02 Å displacements in $\pm x$, $\pm y$ and $\pm z$ directions is around -0.10 (-0.13) eV Å^{-1} in each direction. The results provide clear evidence that the Ge lattice is more flexible than the Si lattice thus able to expand with less associated resistance.

Besides host lattice flexibility, we find that the Li bonding interaction varies substantially as the host material changes, based on the following analysis of density of states (DOS) and charge density distributions. The DOS plot for the Li/Si system [Fig. 2(a) left panel] shows a shift of the Fermi level above the conduction band minimum of Si, indicating the charge transfer from Li to the c-Si host matrix. In addition, we can notice significant overlap between the Li $2sp^3$ and Si $3sp^3$ states in the energy range of -5.5 eV to -1.5 eV, indicating a markable degree of covalency of the Li−Si bonds. As shown in Fig. 2(a) (right panel), this is also well supported by the isosurface plot of charge density differences ($\Delta\rho$) before and after the Li insertion; that is, the charge accumulation in the region between Li and each of its four nearest Si neighbors with a slight shift towards Si suggesting that the Li−Si bonding has polar covalent character.

The DOS and $\Delta\rho$ analyses for the Li/Ge system are overall similar to the Li/Si case but with a few exceptions to distinguish their bonding properties. Firstly, as shown in Fig. 2(b) left panel, the Ge $4sp^3$ peak is relatively narrower as compared to the Si $3sp^3$ case, which is apparently due to the relatively weaker Ge−Ge bonding interaction than the Si−Si interaction as consistent with the result from the aforementioned restoring force analysis. Secondly, the Li $2sp^3$ peak is noticeably smaller in the Li/Ge system (as compared to that in the Li/Si system), suggesting the weaker hybridization between the Li $2sp^3$ and Ge $4sp^3$ orbitals; this is also consistent with the smaller isosurface volume of $\Delta\rho$ with more prominent shift towards Ge [Fig. 2(b) right panel]. The smaller degree of covalency in the Li−Ge bond relative to the Li−Si bond may allow Li to move more easily; indeed, the restoring force experienced by a Li atom displaced from its equilibrium T-site by 0.02 Å in $\pm x$, $\pm y$ and $\pm z$ directions is predicted to be about 50% smaller than that in c-Si [Table S3].

We further examined the interplay between lattice flexibility and bonding interaction by applying hydrostatic strains. The lattice constant of c-Si was made identical to that of c-Ge, and vice versa, causing 5.86% tensile and 5.86% compressive strains, respectively. Here, we will only elaborate on the changes in tensile-strained c-Si since the same explanation can be applied to the Li/Ge case under compression. For c-Si under tension ($a = 5.777$ Å), as the overlap of the sp^3 hybrid orbitals decreases with elongated Si−Si bonds [Fig. 2(c)], so goes the bond rigidity as reflected by the smaller restoring force (-0.09 eV Å^{-1} in x, y and z-directions) [Table S2]. Likewise, hybridization between the Li $2sp^3$ and Si $3sp^3$ states also tends to become weaker with the increased Li−Si distance, as evidenced by the reduced and narrowing Li $2sp^3$ DOS peak as well as the lessening $\Delta\rho$ isosurface volume. As the result, the restoring force
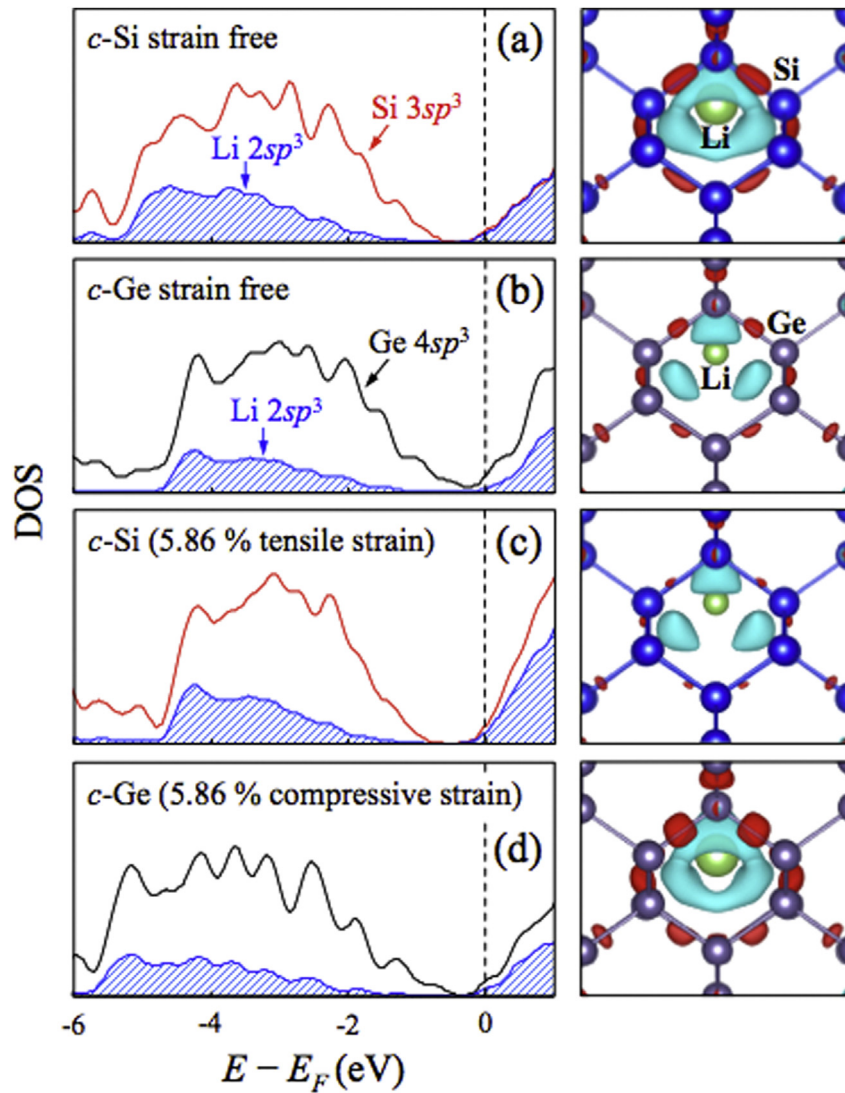
Fig. 2. [Left panel] Electron density of states (DOS) projected on Li and its four nearest Si (or Ge) neighbors in c-Si (or c-Ge); the intensity of Li $2sp^3$ DOS is scaled by 4 times. The vertical dotted line indicates the Fermi level position. [Right panel] Charge density difference ($\Delta\rho$) plots before and after Li insertion; the red and cyan isosurfaces represent the regions of charge gain ($+0.0025$ e Å^{-3}) and loss (-0.0018 e Å^{-3}), respectively. (For interpretation of the references to color in this figure legend, the reader is referred to the web version of this article.)

experienced by the displaced Li atom (0.02 Å in $\pm x$, $\pm y$ and $\pm z$ directions) is found to decrease by approximately 50% as compared to the strain free case [Table S3]. While c-Si may become more Ge-like under tension, the E_a for Li diffusion is reduced to a comparable value (0.37 eV) to that in c-Ge (0.44 eV). Contrarily, the opposite effects are true for c-Ge under compression ($a = 5.457$ Å) [Fig. 2(d)]; that is c-Ge becomes more Si-like due to the increased Ge–Ge bond rigidity and enhanced Li–Ge interaction. The E_a value in c-Ge is found to increase from 0.44 eV at the strain-free state to 0.61 eV under compression, which is remarkably close to the value in c-Si (0.62 eV). These findings demonstrate that Li diffusion is subject to lattice rigidity as well as its interaction with host atoms; between c-Si and c-Ge, a Li atom can migrate more easily (lower E_a) in the later apparently due to the more flexible lattice and weaker Li–Ge interaction.

3.2. Dynamic behavior in lithiated a-Li$_{0.14}$Si and a-Li$_{0.14}$Ge at finite temperatures

As presented earlier, our AIMD simulations show D_{Li} values are significantly different in Ge and Si during early stages of lithiation,

but with increasing Li contents, D_{Li} become progressively more alike. For instance, D_{Li} in a-Li$_{0.14}$Ge is predicted to be 8.23×10^{-7} cm^2 s^{-1} at room temperature while that in a-Li$_{0.14}$Si is five orders of magnitude smaller around 1.60×10^{-12} cm^2 s^{-1}. In addition, we can see that D_{Ge} is about ten orders of magnitude larger than D_{Si}, marking the distinctly different behaviors of a-Si and a-Ge matrices particularly during early stages of lithiation. Therefore, to better understand the underlying reason for the significantly enhanced D_{Li} and D_{Ge}, we analyzed the dynamic behavior of host lattice atoms.

Fig. 3(a) shows AIMD snapshots of the a-Li$_{0.14}$Si and a-Li$_{0.14}$Ge systems annealed at 800 K; the annealing temperature was chosen so that the provided thermal energy can be sufficient to agitate atomic movements but not enough to melt the lattices. In each alloy, we randomly selected a host atom (labeled as 'Si$_A$' and 'Ge$_A$' in red color) and tracked its bonded neighbors (marked as 'Si$_B$' and 'Ge$_B$' in blue color). For a time interval of 8 ps, in a-Li$_{0.14}$Si, Si$_A$ tends to remain bonded to the same four Si$_B$ neighbors, suggesting that the a-Si host network is nearly stationary, barely rearranges its configuration in response to moving Li atoms. Contrarily, Ge$_A$ in a-
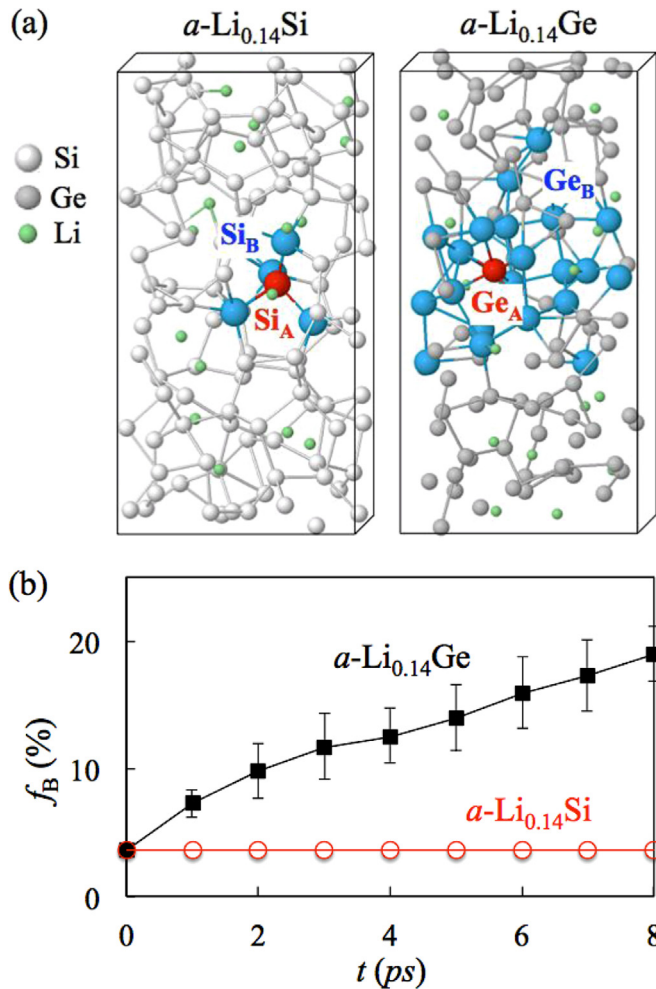
(a)

(b)

Fig. 3. (a) AIMD snapshots of *a*-Li$_{0.14}$Si and *a*-Li$_{0.14}$Ge annealed at 800 K; the host atom of interest is labeled as 'Si$_A$' and 'Ge$_A$' in red color, and the host atoms involved in atomic rearrangement during a time interval of 8 ps are marked as 'Si$_B$' and 'Ge$_B$' in blue color. (b) The extent of atomic rearrangement (quantified by f_B) as a function of MD duration; here, f_B is the averaged number of Si$_B$ (Ge$_B$) neighbors normalized with respect to total number of host atoms within the supercell. (For interpretation of the references to color in this figure legend, the reader is referred to the web version of this article.)

Li$_{0.14}$Ge is found to undergo migration through a series of bond breaking, bond switching, and new bond forming events. The atomic rearrangements associated with Ge$_A$ extends far beyond the initial adjacent neighbors, indicating a significant weakening of the Ge lattice even at the small degree of Li incorporation, which in turn allows facile self-diffusion. To quantify the extent of the atomic rearrangements, the averaged number of Si$_B$ (Ge$_B$) neighbors normalized with respect to total number of host atoms (f_B) within the supercell is plotted as a function of MD duration in Fig. 3(b); these analyses were repeated multiple times on three independently constructed 128-atom supercells. For the system size and MD duration considered here, on average, a Ge atom in *a*-Li$_{0.14}$Ge is estimated to break and form Ge–Ge bonds with approximately 20% of the host atoms while that pertain to the *a*-Si host is only around 4%.

As a result of the facile atomic rearrangements, D_{Ge} is orders of magnitude larger than D_{Si} and consequently leads to faster Li diffusion. Furthermore, the dissimilar dynamic behaviors discussed here may help explaining the different mechanical responses in Si and Ge nanowire (NW) lithiation/delithiation experiments [24];

that is (i) upon lithiation, Si shows high anisotropy with the fastest and most favorable lithiation on {110} planes while Ge undergoes nearly isotropic lithiation, and (ii) upon delithiation, there is apparent crack formation near the center (along axial direction) of the SiNW while the GeNW exhibits porous structure instead of cracking. According to our results, with a small degree of Li alloying, the rigid Si lattice may respond with less significant weakening as compared to the Ge lattice, thereby well retains the crystallographic properties of unlithiated planes, leading to a strong orientation dependence of lithiation. Contrarily, Ge shows pronounced lattice weakening even at low Li concentrations, such that upon lithiation, the original crystallographic characteristic is overshadowed by the sufficiently fast host atom rearrangements, thereby resulting in the isotropic lithiation. Likewise, since Ge is able to easily undergo atomic rearrangements, the matrix is more flexibly adjusted to the large strain variation during Li insertion/extraction and could subsequently reduce crack formation.

Next, we looked into potentially important factors that can influence the dynamic behavior of Ge and thereby Li atoms. As pointed out in our previous study on *a*-Li$_x$Ge alloys [31], the charge transferred from Li can fill the Ge antibonding states, leading to weakened and elongated Ge–Ge bonds, which are anticipated to have non-trivial impacts on Ge atomic rearrangements; in addition, the presence of fast diffusing Li atoms can also affect the Ge dynamic behavior. To assess the relative contribution from each factor, we calculated and compared D_{Ge} values under four different scenarios as listed in Fig. 4: (a) 128-atom pristine *a*-Ge lattice with a calculated mass density of $\rho_{Ge} = 4.87$ g cm^{-3} for reference, (b) porous 112-atom *a*-Ge lattice ($\rho_{Ge} = 4.79$ g cm^{-3}), simulating the lattice expansion/weakening effect associated with elongated Ge–Ge bonds (note that 16 Li atoms, which render a lithiated composition of *a*-Li$_{0.14}$Ge, are removed from the system), (c) negatively charged 112-atom porous *a*-Ge lattice (with 16 additional electrons; $\rho_{Ge} = 4.79$ g cm^{-3}), simulating both the lattice expansion and electron injection effects, and (d) 128-atom *a*-Li$_{0.14}$Ge ($\rho_{Ge} = 4.79$ g cm^{-3}), representing the full effects of Li incorporation; that is, the Ge dynamic behavior is also influenced by the presence of fast diffusing Li atoms as well as the contributions from lattice expansion and electron injection.

AIMD simulations were performed at 700 K to calculate D_{Ge} in these four scenarios. In comparison to pristine *a*-Ge ($D_{Ge} \approx 1.6 \times 10^{-7}$ cm^2 s^{-1}), the porous *a*-Ge is predicted to have a higher D_{Ge} ($\approx 4.6 \times 10^{-6}$ cm^2 s^{-1}), indicating the lattice expansion/weakening effect tends to assist Ge self-diffusion since the elongated Ge–Ge bonds are weaker thus able to rearrange more easily. With the electron injection, the Ge–Ge bonds are further weakened, and D_{Ge} is raised to 7.7×10^{-6} cm^2 s^{-1}. Nevertheless, D_{Ge} is still much greater ($\approx 4.0 \times 10^{-5}$ cm^2 s^{-1}) at the presence of Li atoms in *a*-Li$_{0.14}$Ge, suggesting that the facile rearrangements of host atoms are likely synergistically affected by fast diffusing Li atoms.

Lastly, we examined the effect of Si–Ge alloying on Li diffusivity. The *a*-Li$_{0.14}$Si$_{1-y}$Ge$_y$ alloys of varying Ge contents y (generated based on AIMD simulations) are homogeneous with Li atoms being well dispersed in the matrices, which is consistent with experimental observations that Si and Ge are miscible over the entire composition range and both are able to form favorable alloys with Li [46,47]. The predicted D_{Li}, D_{Si}, and D_{Ge} at 800 K as a function of y are shown in Fig. 5; D_{Li} as well as D_{Si} and D_{Ge} tend to rise monotonically with increasing y, exhibiting a nearly linear relation. As Si–Si bonds are replaced with either relatively weaker Si–Ge or Ge–Ge bonds, the host matrix becomes more flexible and easily undergoes atomic rearrangements, thereby resulting in the enhanced Li diffusivity. While the dynamic behavior of the host lattice is modified through Ge-alloying, we anticipate that the facile atomic rearrangement not only can improve Li diffusivity, but also
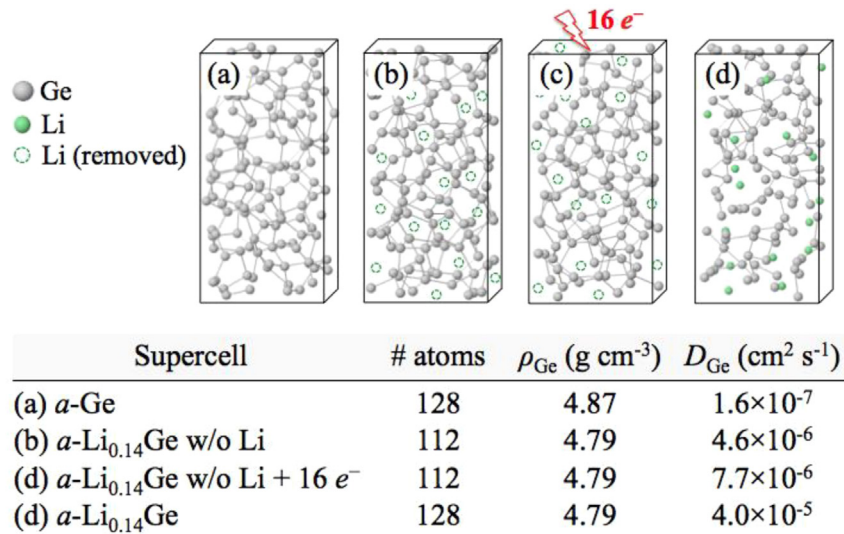
Fig. 4. Schematic illustration of four different simulation scenarios to examine how self-diffusivity (D_{Ge}) is affected by the (b) lattice expansion/weakening, (c) electron injection, and (d) Li-induced combined synergistic effects, as compared to the pure a-Ge case [(a)], together with the predicted D_{Ge} values at 700 K in the lower panel. The total number of atoms and corresponding Ge density (ρ_{Ge}) for each system are also specified.
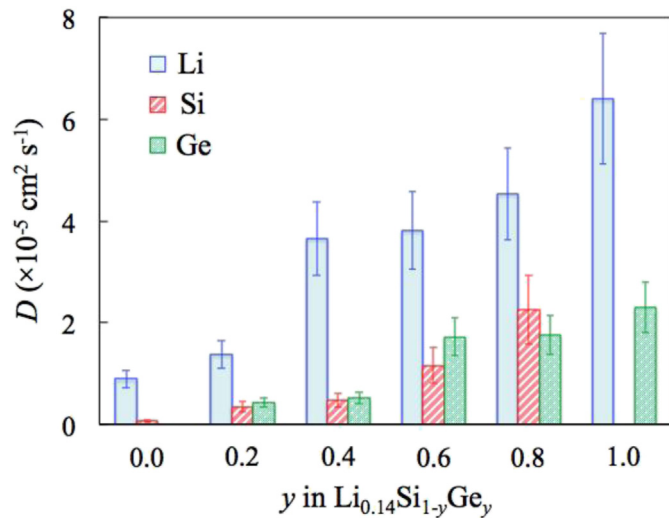

Fig. 5. Predicted diffusivities for Li, Si, and Ge atoms in selected a-Li$_{0.14}$Si$_{1-y}$Ge$_y$ alloys from AIMD simulations at 800 K.

contribute to better strain accommodation, which highlights an important prospect of utilizing Si–Ge alloy as an anode material. Due to the intrinsically lower gravimetric lithiation capacity (of Ge), for Si–Ge alloy anodes, the enhanced Li diffusivity is often at the expense of reduced initial capacity. However, our findings point out that while Si–Ge alloy anodes may have a lower initial capacity, the improved strain accommodation would result in better capacity retention and thus the superior overall cycling performance/ Coulomb efficiency; such that beyond a certain number of charge cycles, Si–Ge alloys anodes due to better capacity retention can exhibit higher capacity than pure Si anodes. That is rapid charging rate and high-capacity retention can be achieved simultaneously via fine-tuning of the Si–Ge alloying condition (composition ratio and spatial distribution).

4. Conclusion

We examined and compared the dynamic lithiation processes in Si and Ge using DFT calculations. The variations of room-

temperature Li diffusivity (D_{Li}) with Li content (x) in a-Li$_x$Si and a-Li$_x$Ge were evaluated using DFT-based MD simulations. For Li diffusion in the crystalline matrix, D_{Li} is predicted around $\times 10^{-13}$ cm^2 s^{-1} in c-Si and $\times 10^{-11}$ cm^2 s^{-1} in c-Ge. With increasing x, D_{Li} in a-Li$_x$Si tends to rise by orders of magnitude from $\times 10^{-12}$ cm^2 s^{-1} ($x = 0.14$) to $\times 10^{-7}$ cm^2 s^{-1} ($x = 3.57$), whereas D_{Li} in a-Li$_x$Ge exhibits virtually no concentration dependence and remains relatively constant around $\times 10^{-7}$. The extremely facile Li diffusion even at low Li concentrations distinguishes Ge from Si as an anode material; this difference in lithiation behavior between a-Li$_x$Ge and a-Li$_x$Si becomes progressively smaller with increasing Li contents. To understand the underlying reasons, we investigated the Li-host matrix interaction as well as their dynamic behavior especially during early stages of lithiation.

Firstly, we found that in comparison to Si, the Ge lattice is (i) less rigid as Ge–Ge bonds are relatively weaker/less directional than Si–Si bonds, and (ii) interacting less strongly with Li since the degree of covalency for Li–Ge bonds is smaller than that for Li–Si bonds; both factors in turn allow Li to migrate more easily (lower E_a) in c-Ge. Furthermore, by applying 5.86% tensile (compressive) strain to c-Si (c-Ge) while c-Si becomes more Ge-like and vice versa, the E_a values for Li diffusion also become comparable; E_a for c-Si (c-Ge) under zero and 5.86% tensile (compressive) strain are 0.62 (0.44) eV and 0.37 (0.61) eV, respectively. These findings demonstrate that Li diffusion is strongly subject to lattice rigidity as well as its interaction with host atoms. Secondly, in addition to the superior D_{Li} that is five orders of magnitude larger in a-Li$_{0.14}$Ge than a-Li$_{0.14}$Si, we found D_{Ge} to be nearly ten orders greater than D_{Si}, indicating that during early stages of lithiation, the a-Si matrix tends to be stationary relative to the diffusing Li atoms while the a-Ge matrix exhibits comparably facile self-diffusivity. To explain the distinctly different dynamic behaviors of two matrices, a-Li$_{0.14}$Ge and a-Li$_{0.14}$Si were annealed at a slightly elevated temperature (800 K) for 8 ps to facilitate sufficient atomic movements. In comparison to the rather motionless a-Si matrix (each Si atom is bonded with the same four nearest neighbors during the entire MD duration), the atomic rearrangements of a-Ge can extend far beyond the initial adjacent neighbors through a series of bond breaking, bond switching, and new bond forming events, which in turn leads to facile self-diffusion and consequently the larger D_{Li}. Later, we also demonstrated that the prompt rearrangements of Ge

host atoms is a synergistic result from the combined contributions of (i) the weakened Ge—Ge bonds/softened lattice due to the Li incorporation, and (ii) the agitation from the fast diffusing Li atoms. Furthermore, the more flexible and facile rearrangements of Ge lattice (as compared to Si lattice) also render a probable explanation to the different mechanical responses in Si and Ge nanowires; for instance, anisotropic SiNW lithiation versus isotropic GeNW lithiation, and the superior capacity retention of GeNWs.

Lastly, we examined the dynamic behavior of a-$Li_{0.14}Si_{1-y}Ge_y$ alloys to assess the effect of Si—Ge alloying on D_{Li}. While the host lattice is modified through Ge-alloying, D_{Li} as well as D_{Si} and D_{Ge} are significantly enhanced and scale linearly with the increasing Ge content (y). This trend indicates that the rate capability may be appreciably improved via effective Ge alloying. Moreover, since the Si—Ge lattice is more flexible and can undergo faster rearrangements upon lithiation, we expect Si—Ge anodes to outperform pure Si anodes in turns of strain accommodation upon lithiation and thereby the superior capacity retention. Therefore, rapid charging rate and high-capacity retention can be achieved simultaneously via fine-tuning of the alloying conditions (composition ratio and spatial distribution), such that more expensive Ge is effectively utilized while Si-alloying mitigates the cost. The origin and extended impacts of the enhanced diffusivities in Ge and Si—Ge alloys are first brought to light in the present work, and we anticipate the improved understanding on the lithiation dynamics may contribute to the design/development of the next-generation, high-power, and high-energy anodes for LIBs.

Acknowledgments

Appendix A. Supplementary data

Supplementary data related to this article can be found at http://dx.doi.org/10.1016/j.jpowsour.2014.04.011.

References

[1] M. Armand, J.M. Tarascon, Nature 451 (2008) 652–657.
[2] A.S. Arico, P. Bruce, B. Scrosati, J.M. Tarascon, W. Van Schalkwijk, Nat. Mater. 4 (2005) 366–377.
[3] J.-M. Tarascon, Phil. Trans. R. Soc. A 368 (2010) 3227–3241.
[4] R.A. Sharma, R.N. Seefurth, J. Electrochem. Soc. 123 (1976) 1763–1768.
[5] B.A. Boukamp, G.C. Lesh, R.A. Huggins, J. Electrochem. Soc. 128 (1981) 725–729.
[6] J. Graetz, C.C. Ahn, R. Yazami, R. Fultz, J. Electrochem. Soc. 151 (2004) A698–A702.
[7] E.M. Conwell, Proc. Inst. Radio Eng. 40 (1952) 1327–1337.
[8] P. Limthongkul, Y.I. Jang, N.J. Dudney, Y.M. Chiang, Acta Mater. 51 (2003) 1103–1113.
[9] H.J. Jung, M. Park, S.H. Han, H. Lim, S.K. Joo, Solid State Commun. 125 (2003) 387–390.
[10] S. Huang, T. Zhu, J. Power Sources 196 (2011) 3664–3668.
[11] C. Yu, X. Li, T. Ma, J. Rong, R. Zhang, J. Shaffer, Y. An, Q. Liu, B. Wei, H. Jiang, Adv. Energy Mater. 2 (2012) 68–73.
[12] B. Laforge, L. Levan-Jodin, R. Salot, A. Billard, J. Electrochem. Soc. 155 (2008) A181–A188.
[13] B. Gao, S. Sinha, L. Fleming, O. Zhou, Adv. Mater. 31 (2001) 816–819.
[14] J. Graetz, C.C. Ahn, R. Yazami, B. Fultz, Electrochem. Solid State Lett. 6 (2003) A194–A197.
[15] C.K. Chan, H.L. Peng, G. Liu, K. McIlwrath, X.F. Zhang, R.A. Huggins, Y. Cui, Nat. Nanotechnol. 3 (2008) 31–35.
[16] L.F. Cui, R. Ruffo, C.K. Chan, H.L. Peng, Y. Cui, Nano Lett. 9 (2009) 491–495.
[17] H.T. Nguyen, F. Yao, M.R. Zamfir, C. Biswas, K.P. So, Y.H. Lee, S.M. Kim, S.N. Cha, J.M. Kim, D. Pribat, Adv. Energy Mater. 1 (2011) 1154–1161.
[18] C.K. Chan, X.F. Zhang, Y. Cui, Nano Lett. 8 (2008) 307–309.
[19] O. Mao, R.L. Turner, I.A. Courtney, B.D. Fredericksen, M.I. Buckett, L.J. Krause, J.R. Dahn, Electrochem. Solid State Lett. 2 (1999) 3–5.
[20] M.D. Fleischauer, J.M. Topple, J.R. Dahn, Electrochem. Solid State Lett. 8 (2005) A137–A140.
[21] L.Y. Beaulieu, T.D. Hatchard, A. Bonakdarpour, M.D. Fleischauer, J.R. Dahn, J. Electrochem. Soc. 150 (2003) A1457–A1464.
[22] A. Netz, R.A. Huggins, W. Weppner, J. Power Sources 95 (2003) 119–121.
[23] X.H. Liu, S. Huang, S.T. Picraux, J. Li, T. Zhu, J.Y. Huang, Nano Lett. 11 (2011) 3991–3997.
[24] X.H. Liu, Y. Liu, A. Kushima, S. Zhang, T. Zhu, J. Liu, J.Y. Huang, Adv. Energy Mater. 2 (2012) 722–741.
[25] V.L. Chevrier, J.R. Dahn, J. Electrochem. Soc. 157 (2010) A392–A398.
[26] V.L. Chevrier, J.R. Dahn, J. Electrochem. Soc. 156 (2009) A454–A458.
[27] V.L. Chevrier, J.W. Zwanziger, J.R. Dahn, J. Alloys Compd. 496 (2010) 25–36.
[28] Q. Zhang, W. Zhang, W. Wan, Y. Cui, E. Wang, Nano Lett. 10 (2010) 3243–3249.
[29] T.L. Chan, J.R. Chelikowsky, Nano Lett. 10 (2010) 821–825.
[30] M.K.Y. Chan, B.R. Long, A.A. Gewirth, J.P. Greeley, J. Phys. Chem. Lett. 2 (2011) 3092–3095.
[31] C.-Y. Chou, H. Kim, G.S. Hwang, J. Phys. Chem. C 115 (2011) 20018–20026.
[32] S.C. Jung, K.-K. Han, Phys. Chem. Chem. Phys. 15 (2013) 13586–13592.
[33] P.E. Blöchl, Phys. Rev. B 50 (1994) 17953–17979.
[34] G. Kresse, J. Hafner, Phys. Rev. B 47 (1993) 558–561.
[35] G. Kresse, J. Furthmuller, Comput. Mater. Sci. 6 (1996) 15–50.
[36] G. Kresse, J. Furthmuller, Phys. Rev. B 54 (1996) 11169–11186.
[37] H.J. Monkhorst, J.D. Pack, Phys. Rev. B 13 (1976) 5188–5192.
[38] S.-H. Lee, G.S. Hwang, J. Chem. Phys. 127 (2007) 224710–224715.
[39] K. Kim, C.-Y. Chou, J.G. Ekerdt, G.S. Hwang, J. Phys. Chem. C 115 (2011) 2514–2521.
[40] C.J. Wen, R.A. Huggins, J. Solid State Chem. 37 (1981) 271–278.
[41] M.R. St. John, A.J. Furgala, A.F. Sammells, J. Electrochem. Soc. 129 (1982) 246–250.
[42] K. Kim, K.E. Kweon, C.-Y. Chou, J.G. Ekerdt, G.S. Hwang, J. Phys. Chem. C 114 (2010) 17942–17946.
[43] V.B. Shenoy, P. Johari, Y. Qi, J. Power Sources 195 (2010) 6825–6830.
[44] X.R. Wang, X. Xiao, Z. Zhang, Surf. Sci. 512 (2002) L361–L366.
[45] Z. Cui, F. Gao, Z. Cui, J. Qu, J. Power Sources 207 (2012) 150–159.
[46] P.R. Abel, A.M. Chockla, Y.-M. Lin, V.C. Holmberg, J.T. Harris, B.A. Korgel, A. Heller, C.B. Mullins, ACS Nano 7 (2013) 2249–2257.
[47] N. Mousseau, M.F. Thorpe, Phys. Rev. B 48 (1993) 5172–5178.